Distinctive structural basis for DNA recognition by the fission yeast Zn_2Cys_6 transcription factor Pho7 and its role in phosphate homeostasis

Angad Garg[1], Yehuda Goldgur[2], Beate Schwer[3] and Stewart Shuman[1],*

[1]Molecular Biology Program, Sloan-Kettering Institute, New York, NY 10065, USA, [2]Structural Biology Program, Sloan-Kettering Institute, New York, NY 10065, USA and [3]Department of Microbiology and Immunology, Weill Cornell Medical College, New York, NY 10065, USA

ABSTRACT

Pho7, a member of the Zn_2Cys_6 family of fungal transcription factors, is the key transcriptional activator underlying fission yeast phosphate homeostasis, a physiological response to phosphate starvation in which the *pho1*, *pho84* and *tgp1* genes are upregulated. Here, we delineated a minimized 61-amino-acid Pho7 DNA-binding domain (DBD) and determined the 1.7 Å crystal structure of the DBD at its target site in the *tgp1* promoter. Two distinctive features of the Pho7 DBD are: it binds DNA as a monomer, unlike most other fungal zinc-cluster factors that bind as homodimers; and it makes extensive interactions with its asymmetric target sequence over a 14-bp footprint that entails hydrogen bonding to 13 individual bases within, and remote from, the CGG triplet typically recognized by other Zn_2Cys_6 DBDs. Base pair substitutions at Pho7 sites in the *tgp1* and *pho1* promoters highlight the importance of the 5′-CGG triplet for Pho7 binding *in vitro* and Pho7-dependent gene expression *in vivo*. We identify several DBD amino acids at which alanine substitution effaced or attenuated the *pho1* phosphate starvation response and concordantly reduced Pho7 binding to a *pho1* promoter site.

INTRODUCTION

Cells respond to phosphate starvation by inducing the expression of proteins involved in extracellular phosphate mobilization and uptake (1,2). The phosphate regulon in the fission yeast *Schizosaccharomyces pombe* comprises three genes that specify, respectively, a cell surface acid phosphatase Pho1, an inorganic phosphate transporter Pho84, and a glycerophosphate transporter Tgp1 (3). Transcription of these genes is repressed during growth in phosphate-rich medium and de-repressed during phosphate starvation. Expression of the phosphate-regulated genes depends on Pho7 (3–6), a 738-amino acid protein that belongs to the zinc binuclear cluster family of fungal DNA-binding transcription regulators (7). The Zn_2Cys_6 transcription factors are defined by a constellation of six cysteines (highlighted in gold in Figure 1A) that coordinate two zinc atoms. Prior studies showed that replacement of the Pho7 cysteines with alanine effaces the fission yeast phosphate starvation response (6).

We recently demarcated an autonomous DNA-binding domain (DBD) of Pho7, from amino acids 279 to 368, that includes the Zn_2Cys_6 module (Figure 1A). We used the Pho7-DBD in DNase footprinting and electrophoretic mobility shift assays (EMSA) to locate Pho7 recognition sites in the promoters of the *pho1* and *tgp1* genes to a 12-nucleotide motif 5′-TCG(G/C)(A/T)xxTTxAA (6). We independently identified the same motif as a Pho7 recognition element via *in silico* analysis of available genome-wide Pho7 ChIP-seq data (3,6). The *pho1* promoter contains two Pho7 12-mer recognition elements (sites 1 and 2), in direct repeat orientation and separated by a 20-nucleotide spacer. The Pho7-DBD binds independently and non-cooperatively to these two sites in the *pho1* promoter. By contrast, the *tgp1* promoter contains a single Pho7 binding site.

The Pho7 DNA recognition site 5′-TCG(G/C)(A/T)xxTTxAA differs from those of other well-studied fungal Zn_2Cys_6 proteins (e.g. Gal4, Leu3, Hap1, Put3, Ppr1), which typically recognize pairs of CGG triplets that are arranged as inverted, direct or everted repeats (7–13). The fungal Zn_2Cys_6 proteins that bind to such DNA elements typically do so as homodimers in which the zinc-binding module confers DNA sequence recognition and a downstream α-helix forms a coiled-coil dimer interface. The *pho1* promoter site 2 (TCGGAAATTAAA) and *tgp1* promoter site (TCGGACATTCAA) that are recognized by Pho7 contain a single CGG triplet. The lack of internal symmetry in the Pho7 DNA binding site raises the prospects that: (i) it might have a unique binding

*To whom correspondence should be addressed. Tel: +1 212 639 7145; Email: s-shuman@ski.mskcc.org
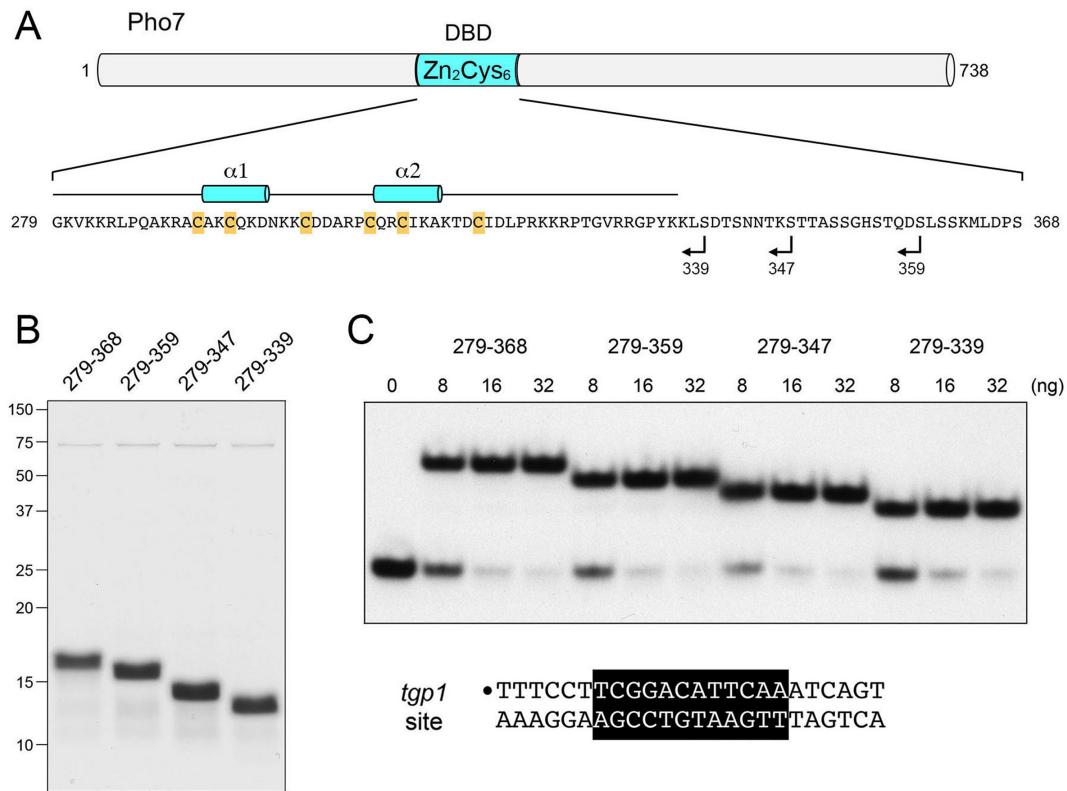
Figure 1. Pho7 DNA binding domain. (**A**) The 738-aa Pho7 polypeptide is depicted as a gray cylinder, with the position of the Zn_2Cys_6 DNA binding domain (DBD; aa 279–368) highlighted in blue. The amino acid sequence of the DBD is shown, with the six zinc-binding cysteines highlighted in gold. The margins of the DBD C-terminal truncations analyzed in the present study are indicated by reverse arrowheads. The secondary structure elements (two α-helices) revealed by the DBD crystal structure are shown above the amino acid sequence. (**B**) Aliquots (5 μg) of the indicated recombinant DBD proteins were analyzed by SDS-PAGE. The Coomassie blue-stained gel is shown. The positions and sizes (in kDa) of marker polypeptides are indicated on the left. (**C**) Truncation defines a minimized DBD. EMSAs were performed using the ^{32}P-labeled *tgp1* promoter DNA probe shown at the bottom. The ^{32}P label is indicated by ●. The Pho7 binding motif is shown in white font on black background. Reaction mixtures (10 μl) containing 0.5 pmol ^{32}P-labeled DNA, 0.34 μg poly(dI-dC), 50 mM NaCl, and 0, 8, 16 or 32 ng Pho7-DBD were incubated for 10 min at room temperature. The mixtures were analyzed by native PAGE in 0.25× TBE. An autoradiograph of the dried gel is shown.

mode in which the component subunits of a homodimer recognize different nucleotide sequence motifs; or (ii) it might bind to DNA as a monomer, *à la* the *Aspergillus* transcription factor AlcR (14).

In order to gain deeper insights into Pho7 specificity, and its role in phosphate homeostasis, we co-crystallized the Pho7 DBD bound to its target DNA element in the *tgp1* promoter and solved the structure of the complex at 1.7 Å resolution. We report that Pho7 binds DNA as a monomer and does so with distinctive features *vis-à-vis* other Zn_2Cys_6 proteins. We educed structure-activity relations *in vitro* and *in vivo* via mutagenesis of the DBD and the *tgp1* and *pho1* promoter elements.

MATERIALS AND METHODS

Pho7 DNA-binding domain

We constructed pET28b-His$_{10}$Smt$_3$-Pho7-DBD plasmids encoding various iterations of the wild-type or alanine-substituted Pho7 DNA binding domain fused to an N-terminal His$_{10}$Smt3 module under the transcriptional control of a T7 RNA polymerase promoter. The plasmids were transfected into *E. coli* BL21(DE3) cells. The procedures

for protein production and purification from soluble bacterial lysates by sequential Ni-affinity chromatography, tag-cleavage, tag-removal via Ni-affinity, and gel-filtration steps were as described previously (6). Protein concentrations were determined as described (6).

DNA binding by EMSA

^{32}P-labeled DNA oligonucleotides (prepared with [γ ^{32}P]ATP and T4 polynucleotide kinase) were annealed to a 2-fold molar excess of a complementary non-labeled DNA oligonucleotide by heating for 10 min at 95°C followed by slow cooling to 25°C. The radiolabeled DNA duplexes were purified by electrophoresis through a native 12% polyacrylamide gel in 0.25xTBE (22 mM Tris-borate, pH 8.3, 0.5 mM EDTA). The labeled DNA was eluted from an excised gel slice, ethanol-precipitated, and resuspended in 10 mM Tris–HCl, pH 7.4, 1 mM EDTA. EMSA reaction mixtures (10 μl) containing 50 mM Tris–HCl, pH 7.4, 10% glycerol, 340 ng poly(dI-dC) (Sigma), 0.24 or 0.5 pmol ^{32}P-labeled DNA, 50 or 200 mM NaCl (final concentration, as specified in figure legends), and 2 μl of Pho7-DBD (serially diluted in buffer containing 50 mM Tris–HCl, pH 7.4, 250 mM NaCl, 10% glycerol, 0.1% Triton X-100

to attain the ng amounts specified in the figures) were incubated for 10 min at 22°C. The mixtures were analyzed by electrophoresis through a native 6% polyacrylamide gel containing 2.5% (v/v) glycerol in 0.25× or 1× TBE buffer. ^{32}P-labeled DNAs (free and Pho7-bound) were visualized by autoradiography. Where indicated, the extent of DNA binding to Pho7 (as a percentage of total DNA in the sample) was determined by scanning the dried gel with a phosphorimager and analyzing the data in ImageQuant.

Crystallization, diffraction data collection, and structure determination

Equimolar concentrations of HPLC-purified 20-mer DNA oligonucleotides 5′-TCCTTCGGACATTCAAATCA and 5′-GATTTGAATGTCCGAAGGAT (from IDT) were annealed by heating for 10 min at 95°C and slow-cooling to room temperature. A protein–DNA mixture containing 0.63 mM Pho7-(279–339), 0.55 mM duplex DNA, 32 mM Tris–HCl, pH 7.4, 125 mM NaCl and 6% glycerol was prepared and incubated at room temperature for 10 min. An aliquot (1 µl) of the protein–DNA solution was then mixed with an equal volume of precipitant solution containing 100 mM Tris–HCl, pH 7.0, 0.2 M sodium acetate, 32.5% PEG-4000. Crystals were grown at room temperature by hanging drop vapor diffusion against the precipitant solution. The crystals were harvested and directly flash-frozen in liquid nitrogen. X-ray diffraction data were collected from single crystals at APS beamline 24ID-C at Zn absorption peak (1.2827 Å) and at APS beamline 24ID-E at 0.97918 Å (remote). The data were integrated with HKL2000 (15). Phases were obtained using multi-wavelength anomalous dispersion (MAD) from two datasets in SHELX (16) to locate two Zn sites. Automated model building was performed by crank2 (CCP4) (17). Interactive model building was done using O (18). Refinement was accomplished with Phenix (19). Data collection and refinement statistics are presented in Supplementary Table S1.

Assay of Pho1 expression

Aliquots of exponentially growing *S. pombe* cultures grown in YES (yeast extract with supplements) medium at 30°C were harvested by centrifugation and the cells were washed with water and suspended in water. For phosphate starvation experiments, the cells were harvested, washed in water, adjusted to A_{600} of ∼0.15 in PMG (Pombe glutamate) medium without phosphate, and then incubated at 30°C for the times specified. To quantify Pho1 acid phosphatase activity, reaction mixtures (200 µl) containing 100 mM sodium acetate (pH 4.2), 10 mM *p*-nitrophenylphosphate, and cells (0.01 to 0.1 A_{600} units) were incubated for 5 min at 30°C. The reactions were quenched by adding 1 ml of 1 M sodium carbonate, the cells were removed by centrifugation, and the absorbance of the supernatant at 410 nm was measured. Acid phosphatase activity is expressed as the ratio of A_{410} (*p*-nitrophenol production) to A_{600} (cells). Each datum is the average (±SEM) of at least three phosphatase assays using cells from three independent cultures.

Allelic exchange of *pho7-Ala* mutants at the *pho7* locus

Replacement of the native *pho7* locus with a *pho7-WT-TAP* or *pho7-Ala-TAP* allele was performed as described previously (6). Correct insertions were verified by Southern blotting and sequencing of PCR-amplified DNA segments to ascertain the presence of the desired allele. To gauge the effect of these mutations on vegetative growth, cultures of *S. pombe* strains containing the indicated *pho7-TAP* allele were grown in liquid medium until A_{600} reached 0.3 to 0.6. The cultures were adjusted to a final A_{600} of 0.1 and aliquots (5 µl) of serial 5-fold dilutions were spotted on YES agar plates, which were then incubated at 20°C, 25°C, 30°C, 34°C and 37°C. To gauge expression of the Pho7 and Pho7-Ala proteins, we performed Western blotting of whole cell extracts of *pho7Δ* and *pho7-TAP* strains grown to mid-log phase in YES medium at 30°C, using a rabbit polyclonal antibody recognizing the TAP tag (Sigma) and rabbit polyclonal anti-Spt5 antibody (20) as a loading control. The procedures for extract preparation and immunoblotting were as described (6).

RESULTS

Defining a minimized DNA binding domain of Pho7

The autonomous Pho7-DBD identified previously (aa 279–368) was serially truncated from the C-terminus in order to demarcate a minimized functional DBD (Figure 1A). Recombinant proteins Pho7-(279–368), Pho7-(279–359), Pho7-(279–347), and Pho7-(279–339) were produced in *E. coli* and purified (Figure 1B). EMSA experiments were performed to gauge their binding to a 5′ ^{32}P-labeled 24-bp DNA duplex comprising the Pho7 site of the *tgp1* promoter (Figure 1C). Each version of the DBD bound to the *tgp1* site to form a single protein–DNA complex of retarded electrophoretic mobility. The distance between the free DNA and the shifted complex correlated with the size of the DBD polypeptide (Figure 1C). The extents of DNA binding to the *tgp1* promoter element as a function of input DBD did not vary between the four DBD constructs tested (Figure 1C), nor did their binding to the site 2 sequence of the *pho1* promoter (not shown). Thus, the 61-aa segment of Pho7 from aa 279 to 339 suffices for DNA binding.

Structure of the Pho7 DBD in complex with its DNA recognition site

Pho7-(279–339) was co-crystallized with a 19-bp DNA duplex (with 3′A and 3′T single-nucleotide overhangs) that corresponds to the Pho7 site of the *tgp1* promoter (Figure 2B). MAD phases from the two Zn atoms were used to solve the structure of the protein–DNA complex at 1.7 Å resolution (R_{work}/R_{free} = 18.8/21.5; Supplementary Table S1). The refined Pho7 protein comprised a continuous polypeptide from Gly279 to Lys336 (denoted by N and C in Figure 2A); the three C-terminal residues were disordered. The six zinc-binding cysteines (Cys292, Cys295, Cys302, Cys308, Cys311, Cys318) are located within and flanking two α-helices (aa 293–298 and 309–314) and a connecting loop (aa 299–308) (Figure 1A). Each zinc atom (green spheres in Figure 2B, with surrounding anomalous difference den-
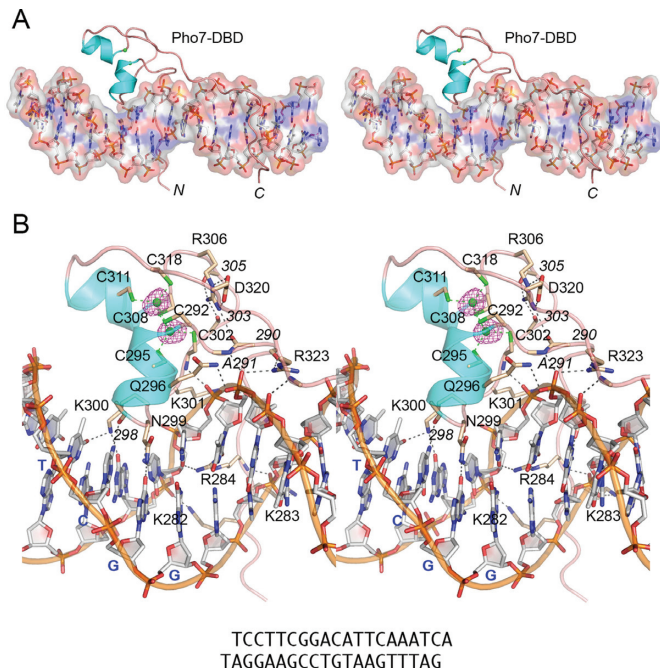
Figure 2. Structure of Pho7 DBD bound to *tgp1* site DNA. (**A**) Global stereo view of the Pho7–DNA complex with the DNA depicted as a stick model, with an overlying transparent surface model to highlight the major and minor grooves. The Pho7 protein is rendered as a cartoon trace with cyan α-helices; the two zinc atoms are shown as green spheres. The N and C termini of the DBD are labeled. (**B**) A detailed stereo view focused on the interactions of the DBD with the DNA major groove over the 5′-TCGG base pairs. The DNA is shown as a stick model with gray carbons and a gold cartoon trace through the backbone phosphates. The 5′-TCGG 'top strand' nucleobases are labeled in blue bold font. Selected amino acids in the DBD are depicted as stick models with beige carbons and labeled in plain black font for side-chains and black italic font for main-chains. Pho7–DNA hydrogen bonds and selected intra-Pho7 hydrogen bonds are indicated by black dashed lines. Cysteine–zinc interactions are denoted by green dashed lines. Anomalous difference density for the zinc atoms, contoured at 4σ, is shown in red mesh.

sity in red mesh) is coordinated tetrahedrally to four cysteines: Zn1 to Cys292, Cys295, Cys302, Cys308; and Zn2 to Cys292, Cys308, Cys311, Cys318 (Figure 2B). The proximal α-helix of the zinc-binding module inserts into the DNA major groove over the 5′-TCG base pairs (Figure 2A and B). The fold of the zinc-binding module is stabilized by a salt-bridge between Arg306 and Asp320 and via hydrogen bonding of Arg306 to the Arg290, Asp303, and Ala305 main-chain carbonyls (Figure 2B). The N-terminal (aa 279–289) and C-terminal (aa 323–336) protein segments flanking the zinc-binding module adopt an extended conformation that drapes continuously over (and penetrates into) the DNA minor groove over an 11-bp span (5′-GGACATTCAAA) (Figure 2A).

The DNA when bound to Pho7-DBD is a B-form helix, but it deviates in conformation from an idealized B-form duplex. Pho7 binding alters the helical axis to elicit a 9° bend (Supplementary Figure S1A) (21). The DNA minor groove widens over the 5′-TTCG and 5′-TCA segments and narrows over the intervening 5′-ACAT segment (Supplementary Figure S1B) (22).

Structural basis for DNA recognition

Pho7 makes an extensive network of amino acid side-chain and main-chain contacts with the DNA nucleobases and backbone phosphates across a 14-bp segment of the *tgp1* promoter, $5'$-$T^1C^2G^3G^4A^5C^6A^7T^8T^9C^{10}A^{11}A^{12}A^{13}T^{14}$ (henceforth numbered starting from the first T nucleotide of the consensus Pho7 binding motif); these are illustrated in two-dimensional cartoon format in Figure 3C, wherein protein-nucleobase interactions are in red font and protein-phosphate contacts are in black font. A detailed stereo view highlighting the Pho7–DNA interface in the major groove over the $5'$-$T^1C^2G^3G^4$ base pairs is shown in Figure 2B. Hydrogen bonding between amino acids and nucleobase edge atoms accounts nicely for Pho7 specificity, as follows. Lys300-Nζ makes bifurcated base-specific contacts to the thymine-O4 atom of the T^1:A pair and the guanine-O6 atom of the C^2:G pair. The Asp298 main-chain carbonyl makes a base-specific hydrogen bond with the cytosine N4 of the C^2:G pair. Asn299-Nδ and the Asn299 main-chain carbonyl make base-specific hydrogen bonds to the guanine-O6 and cytosine-N4 atoms of the G^3:C pair, respectively (Figure 2B). Phosphate hydrogen bonds to this major groove segment are made by Gln296-Nε and the Cys302 main-chain amide (Figure 2B).
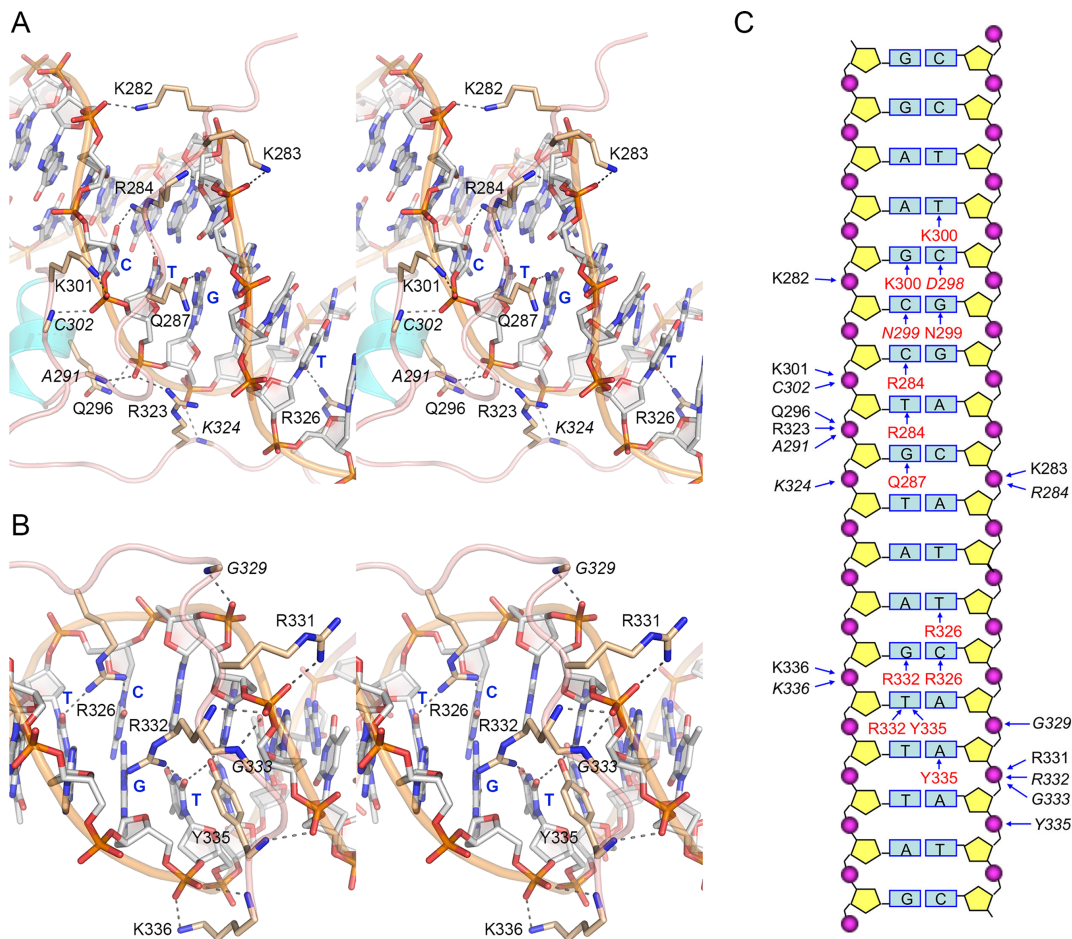
A stereo view of the minor groove interface, focusing on the $5'$-$G^4A^5C^6$ base pairs, is shown in Figure 3A. Here we see that the Arg284 side chain penetrates the narrow minor groove to make bidentate hydrogen bonds with cytosine-O2 of the G^4:C pair and thymine-O2 of the A^5:T pair. These interactions of Arg284 are seemingly pyrimidine-specific and thus favor a Pu:Pyr base pair at the fourth and fifth positions of the Pho7 consensus binding motif (6). Gln287 also penetrates the minor groove to make a hydrogen bond from Oε to guanine-N2 of the C^6:G pair (Figure 3A). Pho7 makes multiple hydrogen bonds to the minor groove phosphates on both strands of this DNA segment. The extended N-terminal polypeptide of the DBD interacts with the phosphates via Lys282-Nζ, Lys283-Nζ, Lys301-Nζ, and the main-chain amides of Arg284, Ala291 and Cys302 (Figure 3A). The extended C-terminal polypeptide contacts the phosphates through hydrogen bonds from the Arg323 side chain and the Lys324 main-chain amide (Figure 3A).

The minor groove interface over the $5'$-$T^9C^{10}A^{11}A^{12}A^{13}$ base pairs (Figure 3B) highlights multiple protein-nucleobase contacts. Arg326 makes bidentate hydrogen bonds with thymine-O2 of the T^9:A pair and cytosine-O2 of the C^{10}:G pair. Arg332 makes bidentate hydrogen bonds with guanine-N3 of the C^{10}:G pair and thymine-O2 of the A^{11}:T pair. The Tyr335-OH makes bifurcated hydrogen bonds to thymine-O2 of the A^{11}:T pair and adenine-N3 of the A^{12}:T pair (Figure 3B). Backbone phosphates on the minor groove are engaged by hydrogen bonds from the Lys336 and Arg331 side chains, the main-chain amides of Gly329, Arg332, Gly333, Tyr335, Lys336 (Figure 3B).

Effect of CGG triplet mutations on Pho7-DBD binding to the *tgp1* promoter *in vitro*

As with other structurally characterized fungal Zn_2Cys_6 DBDs, a CGG base pair triplet is a predominant recipient of Pho7's base-specific interactions with its target site.

Figure 3. The Pho7–DNA interface. (**A**) Detailed stereo view focused on the interactions of the DBD in the minor groove over the 5′-GAC base pairs. The 3′-CTG 'bottom strand' nucleobases are labeled in blue bold font. (**B**) Detailed stereo view focused on the interactions of the DBD in the minor groove over the 5′-TCAA base pairs. Selected bases are labeled in blue bold font. Pho7–DNA hydrogen bonds are indicated by black dashed lines in panel A and B. (**C**) Cartoon diagram summarizing Pho7–DNA contacts. The DNA is depicted as a two-dimensional base pair ladder with the 'top' (5′-CGG triplet-containing) strand on the right and the complementary bottom strand on the left. Amino acids that contact particular backbone phosphates are labeled to the left and right of the phosphates (depicted as magenta spheres) in plain black font for side-chain phosphate contacts and italic black font for main-chain phosphate contacts, as indicated by the arrows pointing at the phosphates. Amino acids that contact particular nucleobases are labeled in red font (plain for protein side-chain interactions with bases and italics for main-chain contacts), as indicated by the arrows pointing at the bases.

To functionally probe the degree to which these three base pairs dictate binding specificity, we replaced the individual C^2:G, G^3:C, and G^4:C pairs with all other standard base pairs (three per position) in the context of the 5′ ^{32}P-labeled 24-bp *tgp1* promoter site probe and assayed them for binding to Pho7-(279-368) DBD, at two levels of input DBD protein, 16 ng and 32 ng, that sufficed to bind 55% and 81% of the DNA probe with the wild-type CGG triplet, respectively (Figure 4A). Replacing the C^2:G pair with T:A or G:C abolished binding to Pho7, while the A:T substitution reduced binding by 17-fold (Figure 4A). The crystal structure suggests that a T^2:A pair would result in unfavorable (repulsive) placement of the Asp298 main chain carbonyl near thymine-O4 and of Lys300-Nζ near adenine-N6 (Figure 2B). In the same vein, a G^2:C pair would unfavorably place the Asp298 main chain carbonyl near guanine-O6 or -N7 and Lys300-Nζ near cytosine-N4. By contrast, the structure seems potentially tolerant (at reduced affinity) of a A^2:T pair, insofar as the Lys300 might be able to adjust its position to form a hydrogen bond with thymine-O4 (Figure 2B).

Mutating the G^3:C pair to A:T, or C:G eliminated Pho7 binding, whereas the T:A substitution reduced binding by 6-fold (Figure 4A). Here also, the crystal structure rationalizes these effects. To wit, an A^3:T pair would cause unfavorable (repulsive) proximity of Asn299-Nδ to adenine-N6 and the Asn299 main-chain carbonyl to thymine-O4, just as a C^3:G pair would place Asn299-Nδ near cytosine-N4 and the Asn299 main-chain carbonyl near guanine-O6 or -N7 (Figure 2B). However, the structure suggest how a T^3:A pair might sustain some binding to Pho7 if Asn299-Nδ donates a hydrogen bond to the thymine-O4.

Changing the G^4:C pair to A:T effaced Pho7 binding but the C:G and T:A mutations elicited 3-fold and 4-fold binding decrements, respectively (Figure 4A). The comparatively modest effect of the C^4:G change is consistent with the fact that the site 1 Pho7 binding element in the *pho1* promoter (5′-TCGCTGCTTGAA) naturally has a CGC triplet
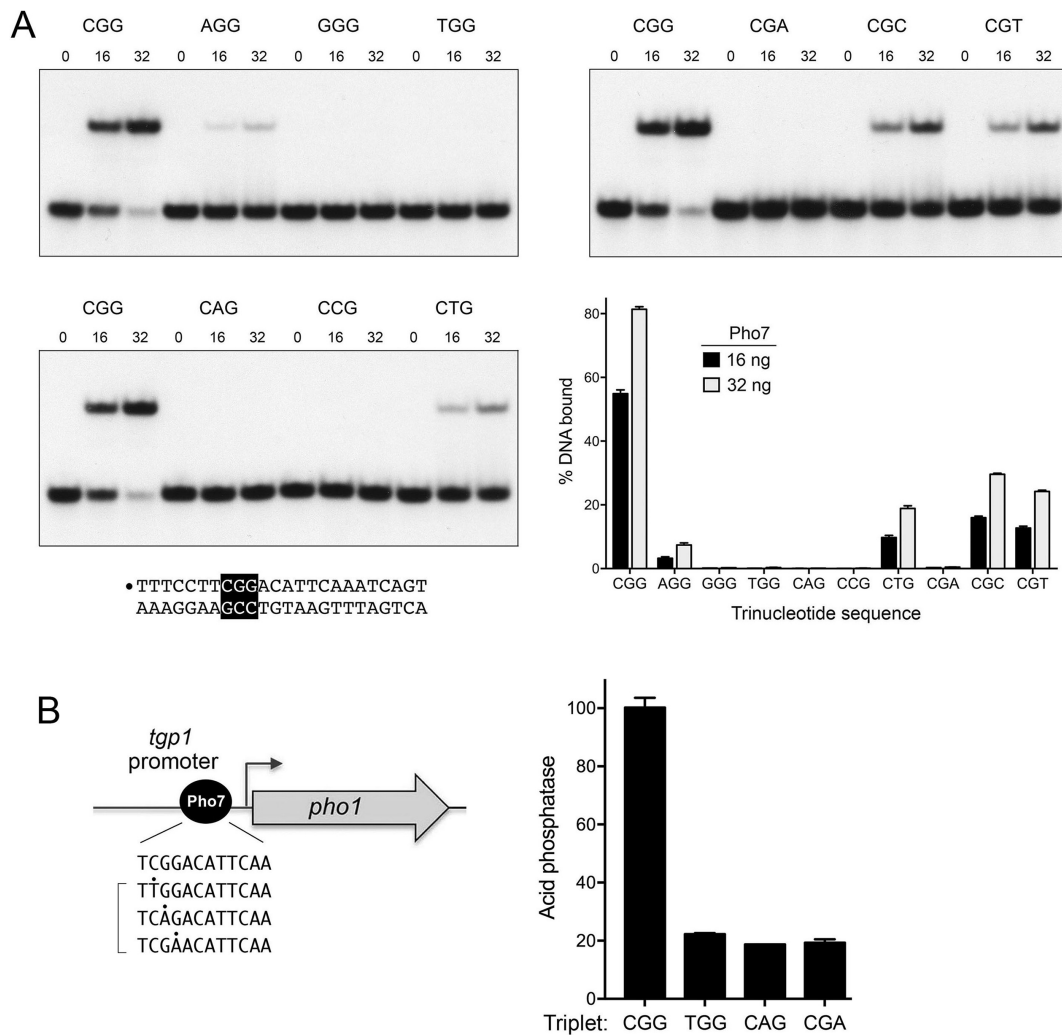
Figure 4. Effect of CGG triplet mutations on Pho7-DBD binding to the *tgp1* promoter *in vitro* and promoter activity *in vivo*. (**A**) The 24-bp *tgp1* promoter DNA is shown at bottom left with the CGG triplet highlighted in white font on black background. The 5′ ³²P-label on the top strand is indicated by ●. Single base pair changes at each position of the CGG triplet were introduced into the 24-bp DNA as specified. Reaction mixtures (10 μl) containing 0.5 pmol ³²P-labeled DNA, 50 mM NaCl, 0.34 μg poly(dI●dC), and 0, 16 or 32 ng of Pho7 DBD were incubated for 10 min at room temperature. The mixtures were analyzed by native PAGE in 0.25x TBE. Autoradiographs of the dried gels are shown. The extents of Pho7 binding to each 24-mer DNA were quantified and are plotted in the bar graph at bottom right. Each datum in the graph is the average of three independent binding experiments ± SEM. (**B**) In the *tgp1●pho1* reporter plasmid shown in cartoon form at *left*, the *pho1* ORF is fused immediately downstream of a fragment of genomic DNA encompassing the *tgp1* transcription start (forward arrow) site plus 42 bp of downstream sequence and 871 bp (–871) of upstream *tgp1* sequence. A single binding site for Pho7 (depicted as a black ball) has been mapped in the *tgp1* promoter (6). The 12-nucleotide site is shown below the reporter cartoon, along with three mutated versions of the CGG triplet. *tgp1●pho1* reporter plasmids with wild-type and the mutated Pho7 sites were introduced into a strain deleted for the endogenous *pho1* gene. Plasmid-containing cells were grown logarithmically in YES medium and assayed for acid phosphatase activity (6).

in lieu of CGG and that site 1 has lower affinity for Pho7 than does the *tgp1* site or *pho1* site 2 (6). In this case, it is not obvious from the crystal structure why the A⁴:T change is so deleterious to Pho7 binding, insofar as one would expect Arg284 to still interact with the thymine-O2 in the minor groove.

Effect of CGG site mutations on *tgp1* promoter activity *in vivo*

To interrogate the *tgp1* promoter, we employed a plasmid reporter (23) in which a genomic DNA segment containing nucleotides -871 to +42 of the *tgp1* transcription unit (with +1 being the *tgp1* mRNA start site) was fused to the

pho1 ORF encoding the fission yeast cell-surface acid phosphatase (Figure 4B). This plasmid generated vigorous acid phosphatase activity when introduced into a *pho1Δ* strain (Figure 4B). Acid phosphatase activity is a gauge of Pho1 enzyme level that correlates tightly with *pho1* mRNA level, as assayed by primer extension as well as RT-qPCR, RNA-seq, and northern blotting (4,5,23–26). The Pho7 binding site in the *tgp1* promoter is located between positions –192 and –181 upstream of the *tgp1* transcription initiation site (Figure 4B). Acid phosphatase activity driven by the *tgp1* promoter reporter plasmid was reduced by 85% in a *pho7Δ* strain background (6). To gauge the role of the CGG triplet in *tgp1* promoter activity, we constructed three mutant reporters in which the triplets were changed to TGG,

CAG or CGA (Figure 4B). We showed in the preceding section that these triplet mutations eliminated Pho7–DBD binding *in vitro*. Here we found that acid phosphatase expression from the reporter plasmids with mutant promoter triplets was reduced by 78–81% (Figure 4B), to nearly the same level seen for the wild-type reporter in a *pho7Δ* strain (6). Thus, the CGG triplet is critical for Pho7-dependent transcription driven by the *tgp1* promoter.

Effect of site 1 and site 2 mutations on *pho1* promoter activity *in vivo*

A plasmid-based reporter containing 283-nt of promoter DNA 5′ of the *pho1* transcription start site suffices to drive vigorous expression of Pho1 acid phosphatase in fission yeast *pho1Δ* cells (24). Pho7 binding site 1 ($^{-187}$TCGCTGCTTGAA^{-176}) and site 2 ($^{-155}$TCGGAAATTAAA^{-144}) in the *pho1* promoter were altered in the context of the reporter plasmid so that the CGC triplet of site 1 was changed to CAC and the CGG triplet of site 2 was changed to CAG (Supplementary Figure S2A). The single-nucleotide changes in sites 1 and 2 reduced Pho1 expression by 93% and 97%, respectively (Supplementary Figure S2B). Thus, the triplets in both Pho7 sites are critical for *pho1* promoter activity.

Effect of Pho7 mutations on phosphate homeostasis *in vivo*

We used the crystal structure of the Pho7-DBD•DNA complex to guide an alanine scan of selected amino acids implicated in DNA recognition (Gln287, Gln296, Lys297, Lys300, Lys301, Arg323, Lys324, Arg326, Arg331) or in maintenance of the DBD fold (Arg306, Lys289, Lys313). The alanine mutations were introduced individually into the gene encoding full-length Pho7 and the *pho7-Ala* alleles were exchanged into the chromosomal *pho7+* locus as described previously (6). The *pho7-WT*, *pho7-Ala* and *pho7Δ* strains were spot-tested for growth on YES agar medium (Figure 5A). As noted previously (6), the *pho7Δ* strain grew slower than wild-type at 25°C (as gauged by colony size) and was progressively 'sicker' at higher (30, 34 and 37°C) and lower (20°C) temperatures (Figure 5A). Whereas the *Q287A*, *K289A*, *Q296A*, *K297A*, *K301A*, *K313A*, *K324A* and *R331A* alleles complemented the temperature-sensitive and cold-sensitive phenotypes, the *R306A* and *R326A* mutations phenocopied the *pho7Δ* growth defect (Figure 5A), signifying that Arg306 (which makes a network of fold-stabilizing hydrogen bonds) and Arg326 (which contacts two nucleobases in the target site) are critical for Pho7 function during vegetative growth. The *K300A* and *R323A* alleles partly complemented the *cs* defect but did not rescue the *ts* phenotype (Figure 5A). Western blotting of whole cell extracts of the *pho7-WT*, *pho7-Ala* and *pho7Δ* strains verified that the Pho7 WT and Ala-mutant proteins were present at similar levels (in relation to an Spt5 loading control) and that no Pho7 was detected in the extract from *pho7Δ* cells (Supplementary Figure S3).

The *pho7-WT*, *pho7-Ala* and *pho7Δ* strains were tested for responsiveness to phosphate starvation by assay of Pho1 acid phosphatase activity prior to and 5 h after transfer of the cells from rich medium (+ phosphate) to synthetic medium lacking phosphate (–phosphate). *pho7-WT* cells evinced a 9-fold increase in Pho1 activity (above the + phosphate baseline) after 5 h of starvation (Figure 5B). As expected, *pho7Δ* cells have a lower basal level of acid phosphatase activity under phosphate-replete conditions and manifested no Pho1 induction during phosphate starvation (Figure 5B). The *K300A*, *R306A*, *R323A*, and *R326A* strains had lower basal Pho1 activity and mounted a feeble response to starvation that did not even reach the basal level of Pho1 activity seen in *WT* cells (indicated by asterisks in Figure 5B). Thus, among the twelve alanine mutations tested, these four changes had the greatest effect on phosphate homeostasis. The remaining eight *pho7-Ala* strains (all of which had reduced basal acid phosphatase activity compared to wild-type) responded to phosphate starvation with 10- to 15-fold increases in Pho1 expression (Figure 5B), but did not attain the level seen in wild-type cells after 5 h in phosphate-free medium. We surmise that these alleles are, to varying degrees, hypomorphs.

Three of the *pho7-Ala* strains that showed a range of effects on Pho1 expression in Figure 5B were selected for more detailed analysis of the kinetics of Pho1 induction over a 6-h interval after shift to phosphate-free medium (Figure 5C). Wild-type cells respond to starvation with a progressive time-dependent accumulation of cell-associated acid phosphatase enzyme after a 2-h lag. *pho7-R331A* cells showed an increase in Pho1 activity between 2 and 3 h; however, the slope of the increase was initially shallower (at up to 4 h) than in wild-type cells, though it attained a *WT*-like slope between 5 and 6 h of starvation (Figure 5C). *pho7-K324A* cells had a slightly longer lag before Pho1 started to accumulate, also at a shallow slope (half that of wild-type between 5 and 6 h) (Figure 5C). The most severe effect was seen in *pho7-K300A* cells, which – after a 4-h lag – began to accumulate Pho1 with a very shallow slope (6-fold-less than wild-type) (Figure 5C). These results point to the importance of the contacts of Lys300 to the guanine base in the C^2:G base pair of the DNA target site for Pho7 activity *in vivo*.

Effect of Pho7 mutations on DNA binding *in vitro*

The 12 alanine mutations studied above in the context of full-length Pho7 were introduced into the Pho7-(279–368) DNA binding domain and the recombinant DBDs were produced in *Escherichia coli* and purified (Supplementary Figure S4). To illuminate a biochemical basis for the observed mutational effects on Pho1 expression *in vivo*, we assayed the DBD mutants for binding to Pho7 sites 1 and 2 in the *pho1* promoter, the rationale being that Pho7 binding to both sites is necessary for *pho1* expression (Supplementary Figure S2) and loss of binding to either site 1 or site 2 could account for defective phosphate homeostasis. The EMSAs with site 1 are shown in Figure 6 and quantified in Figure 7A. The results highlight a correlation between defective site 1 binding *in vitro* and Pho1 expression *in vivo*. To wit: the four Ala mutations that severely affected the phosphate starvation response abolished (in the case of K300A, R326A, and R306A) or drastically reduced (R323A) binding of the DBD to the site 1 probe (Figures 6 and 7A). Other
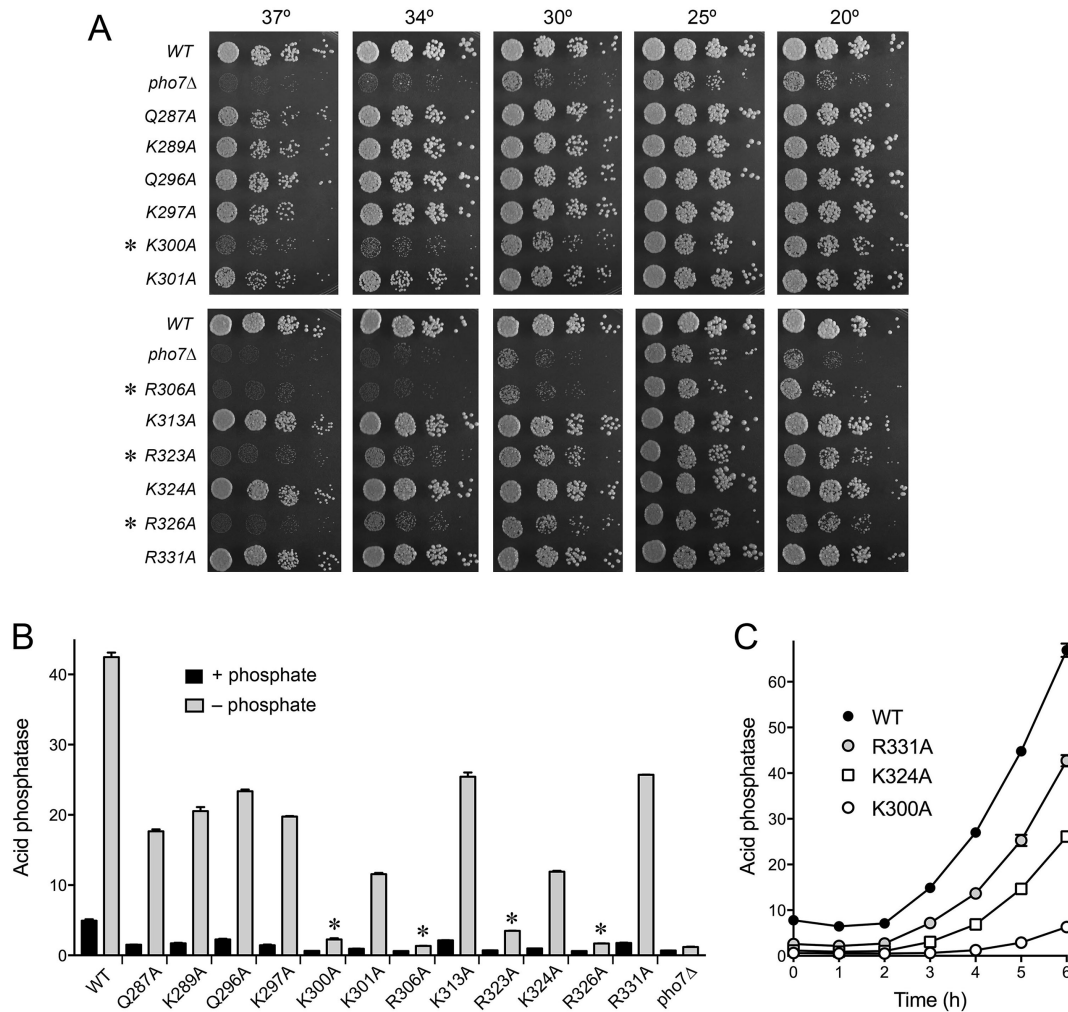
Figure 5. Effect of Pho7 mutations on phosphate homeostasis *in vivo*. (**A**) *S. pombe* strains deleted of *pho7* (*pho7Δ*) or bearing the *pho7* alleles as indicated were spot-tested for growth at the temperatures specified. Alleles that did not complement the temperature-sensitive growth defect of *pho7Δ* are denoted by asterisks. (**B**) Acid phosphatase activity of cells bearing the indicated *pho7* alleles assayed before (+ phosphate) and 5 h after (– phosphate) transfer of logarithmically growing cells to medium lacking phosphate. (**C**) Acid phosphatase activity of cells bearing the indicated *pho7* alleles, plotted as a function of time after transfer to medium lacking phosphate.

mutations either had no effect on site binding (R331A) or reduced site 1 affinity by 2-fold to 8-fold (based on the shifts-to-the right in the DBD titration curves; Figure 7A).
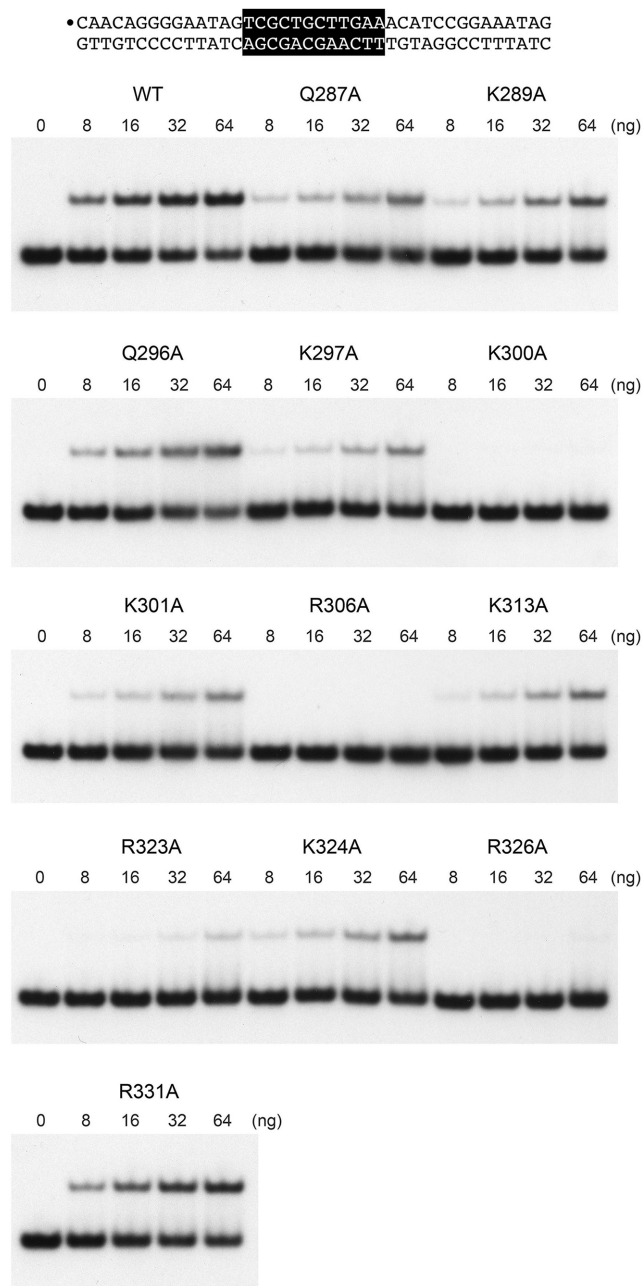
The EMSA results with *pho1* site 2 (shown in Supplementary Figure S5 and quantified in Figure 7B) indicated, as noted previously (6), that the extent of binding was greater for site 2 than site 1 at all DBD concentrations tested. Whereas the R306A mutant was unable to bind site 2, the R326A, K300A, and R323A DBDs (that were defective for site 1 binding) did bind site 2, with affinities within a factor of two of the wild-type DBD. The other Ala mutants bound as well or nearly as well as wild-type to the site 2 probe. These results suggest that Pho7 binding to site 1 in the *pho1* promoter is an Achilles heel with respect to the *pho1* response to phosphate starvation.

Finally, we also gauged mutational effects on DBD binding to the *tgp1* promoter site (EMSAs shown in Supplementary Figure S6 and quantified in Figure 7C). The R306A mutant was unable to bind the *tgp1* DNA. From this and

preceding results, we infer that loss of Arg306 destabilizes the DBD fold and precludes recognition of any of the Pho7 target sites. The other mutations elicited a range of *tgp1* site binding phenotypes; from no effect of R331A (consistent with the *pho1* site 1 and site 2 data) to a sharp decrement (∼16-fold) in the cases of R323A and R326A (consistent with the *pho1* site 1 results).

DISCUSSION

The 738-aa Pho7 protein is the key transcriptional activator underlying fission yeast phosphate homeostasis, a physiological response to phosphate starvation in which the *pho1*, *pho84*, and *tgp1* genes are upregulated. Here, we delineated a minimized 61-aa Pho7 DNA-binding domain (DBD) and determined the atomic structure of the DBD in complex with its target site in the *tgp1* promoter. The structure reveals the basis for target site specificity and highlights distinctive properties and principles of DNA binding by Pho7 *vis à vis* other Zn_2Cys_6 transcription factors. Two features

•CAACAGGGGAATAG<mark>TCGCTGCTTGAA</mark>ACATCCGGAAATAG
GTTGTCCCCTTATC<mark>AGCGACGAACTT</mark>TGTAGGCCTTTATC

Figure 6. Binding of Pho7 mutants to *pho1* promoter site 1. EMSAs were performed using the ^{32}P-labeled site 1 DNA probe shown at the top. The ^{32}P label is indicated by •. The Pho7 binding motif is shown in white font on black background. Reaction mixtures (10 μl) containing 0.24 pmol ^{32}P-labeled DNA, 0.34 μg poly(dI-dC), 50 mM NaCl, and 0, 8, 16, 32 or 64 ng Pho7-DBD were incubated for 10 min at room temperature. The mixtures were analyzed by native PAGE in 0.25× TBE. Autoradiographs of the dried gels are shown.

of Pho7 stand out: (i) it binds DNA as a monomer, unlike most other fungal zinc-cluster factors that bind DNA as homodimers, e.g. Gal4, Leu3, Ppr1, Hap1 and Put3 (8–13); and (ii) it makes contact with its target site over a 14-bp footprint that entails nucleobase contacts remote from the CGG triplet typically recognized by other Zn_2Cys_6 DBDs.

The Pho7 DBD resembles the canonical Gal4 DBD (8,9) with respect to the virtually identical folds of their Zn_2Cys_6 modules and the constituents of their zinc coordination complexes (see Supplementary Figure S7 for a stereo view of the aligned Pho7 and Gal4 modules). In both cases, secondary structure elements in the module are limited to two α-helices (Supplementary Figure S7). The primary structures of the Pho7 and Gal4 modules are similar to the extent of 13 positions of amino acid identity (including the 6 zinc-coordinating cysteines) and 5 positions of side chain similarity across a 44-amino acid protein segment (Supplementary Figure S7).

A vertically offset superposition of the Pho7•DNA and Gal4•DNA complexes with respect to their zinc modules and the 5′-CGG base pair triplet that they recognize in the major groove is shown in Figure 8, in which only one Gal4 protomer of the DNA-bound homodimer is included. The DNA-interacting portions of the Pho7 and Gal4 proteins are colored green and magenta, respectively. The Pho7 DBD, which engages its target DNA as a monomer, has no counterpart of the coiled-coil homodimerization domain at the C-terminus of the Gal4 DBD (colored gray in Figure 8). The only amino acid side chain contact that Gal4 makes to target site nucleobases is a bifurcated hydrogen bond from Lys18-Nζ to the guanine-N7 atom of the second base of the 5′-CG̲G triplet and to the guanine-O6 atom of the third base of the 5′-CGG̲ triplet (8,9). The equivalent residue in Pho7 is Asn299, which donates a hydrogen bond from Nδ to guanine-O6 of the second base of the 5′-CG̲G triplet. The corresponding side chain in other Zn_2Cys_6 transcription factors also makes base-specific DNA interactions to this second guanine; whether from a histidine side chain in the case of Put3 (11), or a lysine side chain in Ppr1, Hap1, Leu3 and AlcR (10,12–14). All of the Zn_2Cys_6 proteins make a pair of hydrogen bonds from adjacent main-chain carbonyls to the cytosine-N4 of the first C:G pair of the triplet and the cytosine-N4 of the second G:C pair: these are the equivalent of the main-chain Pho7•DNA contacts made by Asp298-O and Asn299-O (Figure 2B).

A key difference between the DNA interfaces of Pho7 and Gal4 is that Pho7 makes additional contacts with the nucleobases in the major groove via Lys300 (Figure 2B) that account for Pho7's preference for a 5′-T:A pair preceding the CGG triplet in the consensus Pho7 recognition element (6). Our mutational studies here underscore the importance of Lys300 for Pho7 activity *in vitro* and *in vivo*. An even more striking distinction is that the extended peptide segment in Gal4 downstream of the zinc-binding module (i.e. the linker to the dimerization module) tracks above the minor groove without directly contacting the DNA (Figure 8). By contrast, the homologous segment of Pho7 hugs closely to and penetrates the DNA minor groove, as does the N-terminal peptide preceding the Pho7 zinc-binding module (of which there is no counterpart in the Gal4 structure). These two Pho7 segments make numerous contacts to the backbone phosphates of both DNA strands and to seven of the nucleobases downstream of the 5′-CGG triplet (Figure 3A–C).

The footprint of Pho7–DNA atomic interactions spans 14 nucleotides and entails hydrogen bonding to 13 individual nucleobases by a monomeric DBD. The sequence of the
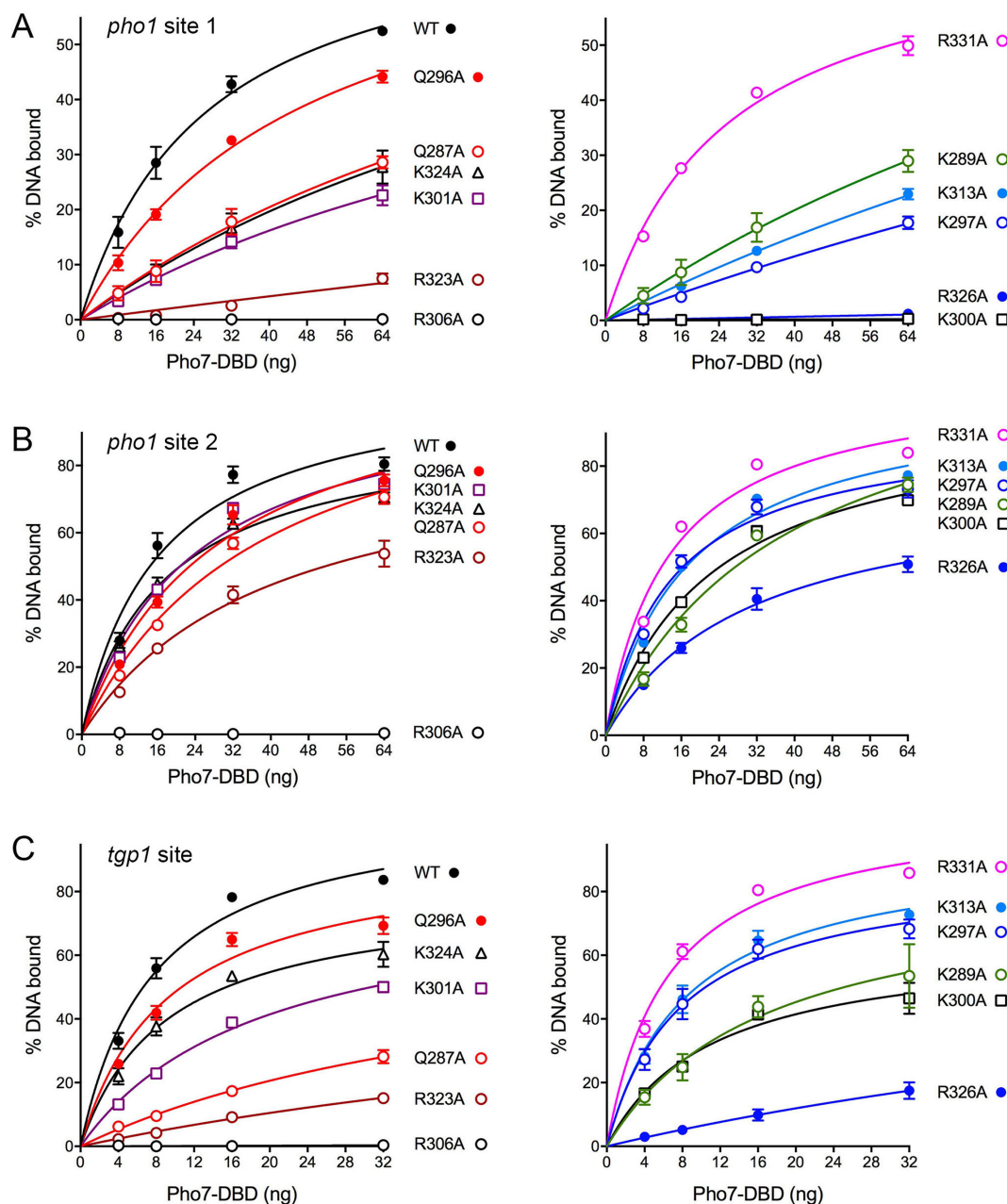
Figure 7. Mutational effects on Pho7 binding to three target sites. EMSAs were performed using the *pho1* site 1 (**A**), *pho1* site 2 (**B**), and *tgp1* site (**C**) DNA probes as described in the legends to Figure 6, Supplementary Figures S5 and S6. The extents of DNA binding were quantified and are plotted as function of input Pho7. For clarity, the WT and mutant binding curves for each site are plotted in two groups in side-by-side graphs. Each datum in the graphs is the average of three independent binding experiments ±SEM.

Pho7 DNA binding site is asymmetric and has only one CGG triplet, in keeping with the monomeric binding mode, as opposed to the DNA sites consisting of two triplets, in various orientations and with variable spacing between them, that are recognized by homodimeric Zn_2Cys_6 transcription factors (7–13). The NMR structure of the Zn_2Cys_6 protein AlcR showed that it bound to DNA as a monomer (14). Yet AlcR's structure and DNA interface differ from Pho7's (see Supplementary Figure S8). For example, the AlcR DBD fold includes two 'extra' α-helices located between and downstream of the zinc-binding α-helices (14)

that have no counterpart in Pho7 (or most other Zn_2Cys_6 proteins). AlcR recognizes a shorter consensus sequence, the pentamer 5′-(A/T)GCGG (27), than does Pho7. The AlcR structure bound to a 10-bp duplex containing this element pinpointed four arginine side chains that make hydrogen bonds to four nucleobases within the consensus pentamer (14), in addition to the lysine cited above that contacts the CGG guanine. The five side chains in AlcR that contact the bases are situated within or upstream of the folded zinc-binding module. Unlike the situation with Pho7, the segment of the AlcR DBD downstream of the last zinc-binding
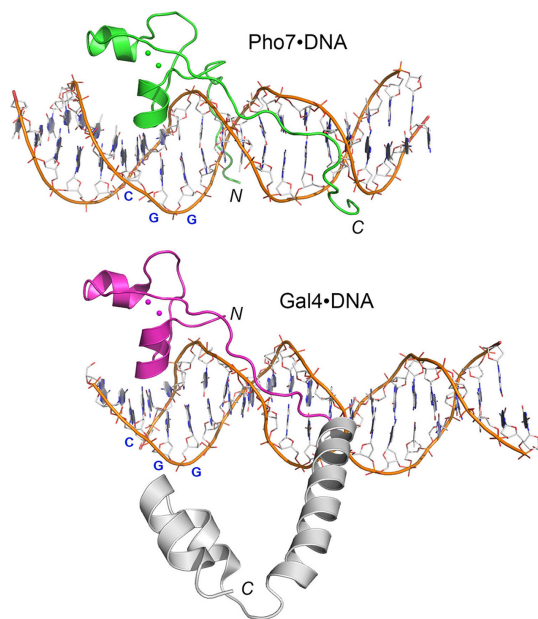
Figure 8. Comparison of Pho7 and Gal4 DNA binding modes. A vertically offset superposition of the Pho7•DNA and Gal4•DNA (pdb: 3COQ) complexes with respect to their zinc modules and the 5′-CGG base pair triplet that they recognize in the major groove is shown. Only one Gal4 protomer of the DNA-bound homodimer is included. The DNA-interacting portions of the Pho7 and Gal4 proteins are colored green and magenta, respectively. The Pho7 DBD has no counterpart of the coiled-coil homodimerization domain at the C-terminus of the Gal4 DBD (colored gray).

cysteine makes no direct contacts with the DNA target site (14).

The functional studies inspired by the Pho7•DNA complex underscore the importance of the 5′-CGG triplet for Pho7 binding *in vitro* and for Pho7-dependent gene expression *in vivo*. One of the triplet mutations that permits lowered affinity binding by Pho7-DBD *in vitro* corresponds to the 5′-CGC variant that is present naturally in Pho7 binding site 1 of the *pho1* promoter (6). Our mutagenesis of Pho7 (though not exhaustive) identifies amino acids at which alanine substitution effaces or strongly attenuates the *pho1* phosphate starvation response *in vivo* and concordantly reduce Pho7 binding *in vitro* to site 1 in the *pho1* promoter. The hierarchy of mutational effects on binding to different promoter elements tested is consistent with site 1 (with its variant CGC triplet) being most sensitive to Pho7 alterations.

In summary, the present study provides a structural framework for understanding Pho7 control of fission yeast phosphate homeostasis, reveals distinctive features of the Pho7–DNA interface, and presages further efforts to delineate how the full-length Pho7 protein activates transcription and responds to regulatory cues.

DATA AVAILABILITY

Coordinates and structure factors have been deposited in the Protein Data Bank under accession code 6E33.

SUPPLEMENTARY DATA

Supplementary Data are available at NAR Online.

REFERENCES

1. Tomar,P. and Sinha,2H. (2014) Conservation of PHO pathway in ascomycetes and the role of Pho84. *J. Biosci.*, **39**, 525–536.
2. Jain,A., Nagarajan,V.K. and Raghothama,K.G. (2012) Transcriptional regulation of phosphate acquisition by higher plants. *Cell. Mol. Life Sci.*, **69**, 3207–3224.
3. Carter-O'Connell,I., Peel,M.T., Wykoff,D.D. and O'Shea,E.K. (2012) Genome-wide characterization of the phosphate starvation response in *Schizosaccharomyces pombe*. *BMC Genomics*, **13**, 697.
4. Henry,T.C., Power,J.E., Kerwin,C.L., Mohammed,A., Weissman,J.S., Cameron,D.M. and Wykoff,D.D. (2011) Systematic screen of *Schizosaccharomyces pombe* deletion collection uncovers parallel evolution of the phosphate signal pathways in yeasts. *Euk. Cell*, **10**, 198–206.
5. Schwer,B., Sanchez,A. and Shuman,S. (2015) RNA polymerase II CTD phospho-sites Ser5 and Ser7 govern phosphate homeostasis in fission yeast. *RNA*, **21**, 1770–1780.
6. Schwer,B., Sanchez,A.M., Garg,A., Chatterjee,D. and Shuman,S. (2017) Defining the DNA binding site recognized by the fission yeast Zn_2Cys_6 transcription factor Pho7 and its role in phosphate homeostasis. *mBio*, **8**, e01218-17.
7. MacPherson,S., Larochelle,M. and Tyrcotte,B. (2006) A fungal family of transcriptional regulators: the zinc cluster proteins. *Microbiol. Mol. Biol. Rev.*, **70**, 583–604.
8. Marmorstein,R, Carey,M, Ptashne,M and Harrison,S.C. (1992) DNA recognition by GAL4: structure of a protein–DNA complex. *Nature*, **356**, 408–414.
9. Hong,M., Fitzgerald,M.X., Harper,S., Luo,C., Speicher,D.W. and Marmorstein,R. (2008) Structural basis for dimerization in DNA recognition by Gal4. *Structure*, **16**, 1019–1026.
10. Marmorstein,R. and Harrison,S.C. (1994) Crystal structure of a PPR1-DNA complex: DNA recognition by proteins containing a Zn_2Cys_6 binuclear cluster. *Genes Dev.*, **8**, 2504–2512.
11. Swaminathan,K., Flynn,P., Reece,R.J. and Marmorstein,R. (1997) Crystal structure of a PUT3-DNA complex reveals a novel mechanism for DNA recognition by a protein containing a Zn_2Cys_6 binuclear cluster. *Nat. Struct. Biol.*, **4**, 751–759.
12. King,D.A., Zhang,L., Guarente,L. and Marmorstein,R. (1999) Structure of a HAP1-DNA complex reveals dramatically asymmetric DNA binding by a homodimeric protein. *Nat. Struct. Biol.*, **6**, 64–71.
13. Fitzgerald,M.X., Rojas,J.R., Kim,J.M., Kohlhaw,G.B. and Marmorstein,R. (2006) Structure of a Leu3-DNA complex: recognition of everted CGG half-sites by a Zn_2Cys_6 binuclear cluster protein. *Structure*, **14**, 725–735.
14. Cahuzac,B., Cerdan,R., Felenbok,B. and Guittet,E. (2001) The solution structure of an AlcR-DNA complex sheds light onto the unique tight and monomeric DNA binding of a Zn_2Cys_6 protein. *Structure*, **9**, 827–836.
15. Otwinowski,Z. and Minor,W. (1997) Processing of X-ray diffraction data collected in oscillation mode. *Methods Enzymol.*, **276**, 307–326.
16. Sheldrick,G.M. (2010) Experimental phasing with SHELXC/D/E: combining chain tracing with density modification. *Acta Crystallogr.*, **D66**, 479–485.

17. Potterton,L., Agirre,J., Ballard,C., Cowtan,K., Dodson,E., Evans,P.R., Jenkins,H.T., Keegan,R., Krissinel,E., Stevenson,K. *et al.* (2018). CCP4i2: the new graphical user interface to the CCP4 program suite. *Acta Crystallogr.*, **D74**, 68–84.

18. Jones,T.A., Zou,J.Y., Cowan,S.W. and Kjeldgaard,M. (1991) Improved methods for building protein models in electron density maps and the location of errors in these models. *Acta Crystallogr.*, **A47**, 110–119.

19. Adams,P.D., Afonine,P.V., Bunkóczi,G., Chen,V.B., Davis,I.W., Echols,N., Headd,J.J., Hung,L.W., Kapral,G.J., Grosse-Kunstleve,R.W. *et al.* (2010) PHENIX: a comprehensive Python-based system for macromolecular structure solution. *Acta Crystallogr.*, **D66**, 213–221.

20. Schwer,B., Schneider,S., Pei,Y., Aronova,A. and Shuman,S. (2009) Characterization of the *Schizosaccharomyces pombe* Spt5-Spt4 complex. *RNA*, **15**, 1241–1250.

21. Blanchet,C., Pasi,M., Zakrzewska,K. and Lavery,R. (2011) CURVES+ web server for analyzing and visualizing the helical, backbone and groove parameters of nucleic acid structures. *Nucleic Acids Res.*, **39**, W68–W73.

22. Lu,X.J. and Olson,W.K. (2003) 3DNA: a software package for the analysis, rebuilding and visualization of three-dimensional nucleic acid structures. *Nucleic Acids Res.*, **31**, 5108–5121.

23. Sanchez,A.M., Shuman,S. and Schwer,B. (2018) Poly(A) site choice and Pol2 CTD Serine-5 status govern lncRNA control of phosphate-responsive *tgp1* gene expression in fission yeast. *RNA*, **24**, 237–250.

24. Chatterjee,D., Sanchez,A.M., Goldgur,Y., Shuman,S. and Schwer,B. (2016) Transcription of lncRNA *prt*, clustered *prt* RNA sites for Mmi1 binding, and RNA polymerase II CTD phospho-sites govern the repression of *pho1* gene expression under phosphate-replete conditions in fission yeast. *RNA*, **22**, 1011–1025.

25. Schwer,B., Bitton,D.A., Sanchez,A.M., Bähler,J. and Shuman,S. (2014) Individual letters of the RNA polymerase II CTD code govern distinct gene expression programs in fission yeast. *Proc. Natl. Acad. Sci. U.S.A.*, **111**, 4185–4190.

26. Garg,A., Sanchez,A.M., Shuman,S. and Schwer,B. (2018) A long noncoding (lnc) RNA governs expression of the phosphate transporter Pho84 in fission yeast and has cascading effects on the flanking *prt* lncRNA and *pho1* genes. *J. Biol. Chem.*, **293**, 4456–4467.

27. Nikolaev,I., Lenouvel,F. and Felenbok,B. (1999) Unique DNA binding specificity of the binuclear zinc AlcR activator of the ethanol utilization pathway in *Aspergillus nidulans*. *J. Biol. Chem.*, **274**, 9795–9802.